



1    **Atmospheric CO<sub>2</sub> inversions at the mesoscale using data driven**  
2    **prior uncertainties. Part1: Methodology and system evaluation**

3

4    Panagiotis Kountouris<sup>1</sup>, Christoph Gerbig<sup>1</sup>, Christian Rödenbeck<sup>1</sup>, Ute Karstens<sup>1,\*</sup>, Thomas F.  
5    Koch<sup>2</sup>, Martin Heimann<sup>1</sup>

6    <sup>1</sup>Max Planck Institute for Biogeochemistry, Jena, Germany

7    <sup>2</sup>Meteorological Observatory Hohenpeissenberg, Deutscher Wetterdienst,  
8    Germany

9    \*Now at ICOS Carbon Portal, Lund University, Lund, Sweden

10

11    *Correspondence to:* P. Kountouris (pkount@bgc-jena.mpg.de)



## 1 Abstract

2 Atmospheric inversions are widely used in the optimization of surface carbon fluxes at regional  
3 scale using information from atmospheric CO<sub>2</sub> dry mole fractions. In many studies the prior flux  
4 uncertainty applied to the inversion schemes does not reflect directly the true flux uncertainties  
5 but it is used in such a way to regularize the inverse problem. Here, we aim to implement an  
6 inversion scheme using the Jena inversion system and applying a prior flux error structure  
7 derived from a model – data residual analysis using high spatial and temporal resolution over a  
8 full year period in the European domain. We analyzed the performance of the inversion system  
9 with a synthetic experiment, where the flux constraint is derived following the same residual  
10 analysis but applied to the model-model mismatch. The synthetic study showed a quite good  
11 agreement between posterior and “true” fluxes at European/Country and annual/monthly scales.  
12 Posterior monthly and country aggregated fluxes improved their correlation coefficient with the  
13 “known truth” by 7% compared to the prior estimates when compared to the reference, with a  
14 mean correlation of 0.92. Respectively, the ratio of the standard deviation between  
15 posterior/reference and prior/reference was also reduced by 33% with a mean value of 1.15. We  
16 identified temporal and spatial scales where the inversion system maximizes the derived  
17 information; monthly temporal scales at around 200 km spatial resolution seem to maximize the  
18 information gain.

19



## 1 **1 Introduction**

2

3 The continuous rise of the abundance of greenhouse gases in the atmosphere, especially due to  
4 fossil fuel combustion, alerted the scientific community to systematically monitor these  
5 emissions. The challenge is not limited only to revealing the spatial distribution of CO<sub>2</sub> sources  
6 and sinks on continental scales, but also to accurately quantifying CO<sub>2</sub> emissions and their  
7 uncertainties at country scales. In situ atmospheric measurements of the atmospheric CO<sub>2</sub>  
8 variability combined with inverse atmospheric models are used as an independent method to  
9 provide “top down” flux estimates for comparison with estimates from “bottom up” methods.  
10 The latter use local observations (e.g. eddy covariance), and combine these with ancillary data,  
11 e.g. soil maps, satellite data, and terrestrial ecosystem models in order to spatially scale up local  
12 flux estimates to larger regions (Jung et al., 2009). Both approaches act complementary, for  
13 optimal comprehension of carbon sources and sinks in a “multiple constraint” (Schulze et al.,  
14 2010) approach and emission inventories assessment. As these inventories are used to deduce  
15 national emission estimates, in compliance with the Kyoto protocol requirements, accuracy is  
16 essential.

17 An atmospheric inverse modeling system provides the link from atmospheric concentrations to  
18 surface fluxes. However, the limited number of observations available for solving the system for  
19 quite a number of unknowns (spatially and temporally resolved fluxes) makes the inverse  
20 problem strongly under-determined. To solve the inverse problem the system incorporates  
21 Bayes’ theorem and uses a-priori knowledge, provided by e.g. biosphere models and emission  
22 inventories accompanied by corresponding uncertainty estimates. Then, the system optimizes the  
23 a-priori fluxes by minimizing the difference between model predictions and observed  
24 concentrations. For the current study only the biospheric fluxes were optimized, and emissions  
25 from fossil fuel combustion are assumed to be known much better, as it is the case in almost all  
26 published regional inversion studies. Inversion systems have been extensively used to derive  
27 spatiotemporal flux patterns at global (e.g. Enting et al., 1995; Kaminski et al., 1999a; Gurney et  
28 al., 2003; Mueller et al., 2008), and regional scale (e.g. Gerbig et al., 2003a; Peylin et al., 2005;  
29 Lauvaux et al., 2012; Broquet et al., 2013).



1 The challenge in regional inversions is to reconstruct at high resolution the spatiotemporal flux  
2 patterns, usually of the net ecosystem exchange (NEE). For that purpose currently deployed  
3 global or regional inverse modeling schemes use different state spaces (i.e. the set of variables to  
4 be optimized through the inversion process). Peters et al. (2007) split the domain of interest into  
5 regions according to ecosystem type. Subsequently fluxes are optimized by using linear  
6 multiplication factors to scale NEE for each week and each region. The pitfall of this system is  
7 that a zero prior flux has no chance to be optimized and remains zero. Zupanski et al. (2007)  
8 divided the NEE into two components, i.e. the gross photosynthetic production (GPP) and  
9 ecosystem respiration (R). Then multiplicative factors for the gross fluxes were derived on the  
10 grid scale, under the assumption of being constant in time. A step further made by Lokupitiya et  
11 al. (2008) used the same approach but with an 8-week time window allowing for temporal  
12 variations for the multiplicative factors. A different approach introducing the carbon cycle data  
13 assimilation system (CCDAS) was implemented by Rayner et al. (2005) and Kaminski et al.  
14 (2012) by constraining global parameters within a biosphere model able to control surface-  
15 atmosphere exchange fluxes, against observed atmospheric CO<sub>2</sub> mole fractions, instead of the  
16 fluxes themselves. Lauvaux et al. (2012) used a Bayesian approach based on matrix inversion,  
17 separately optimizing day and night time fluxes at a weekly time scale for a limited simulation  
18 period and domain. An attempt to assess which of these approaches better reproduces NEE was  
19 made by Tolk et al. (2011). This study investigated the impact of different inversion approaches  
20 via a synthetic experiment utilizing an ensemble Kalman filter technique and the same transport  
21 model for all cases. They found that inversions which separately optimize gross fluxes within a  
22 pixel inversion concept perform better on reconstructing the NEE, although they fail to obtain  
23 the gross fluxes. Taking into consideration these findings we also choose the pixel based  
24 inversions but optimizing the net biogenic fluxes as we are mainly interested in the total carbon  
25 flux budget.

26 Introducing proper prior flux uncertainties is crucial for meaningful posterior estimates, as these  
27 uncertainties weight the prior knowledge between different locations and times, as well as with  
28 respect to the data constraint. The uncertainties have the form of a covariance matrix and can be  
29 categorized in uncertainties of the prior fluxes, and uncertainties of the observational constraint,  
30 which includes measurement and transport model uncertainties. While the observational  
31 constraint may be more easily defined with the main diagonal of the covariance matrix



1 representing the uncertainty of the observations and the model at a specific time and location, our  
2 knowledge for the prior uncertainty is limited. Early inversions assumed fully uncorrelated flux  
3 uncertainties (Kaminski et al., 1999b), while spatial and temporal correlations were used later by  
4 Rödenbeck et al. (2003), who investigated the autocorrelation of monthly CO<sub>2</sub> fluxes calculated  
5 by a set of terrestrial and ocean models. In Rödenbeck (2005), spatial correlations for land fluxes  
6 were assigned to a state space of 4° latitude x 5° longitude resolution. Slightly different  
7 correlation length scales were considered for the meridional and zonal direction, assuming that  
8 the climate zone of the later varies less than of the former. Flux correlations on land were  
9 determined by assuming an exponential pulse response function with a length of 1275 km. This  
10 leads to correlations with approximately twice the correlation length. Typically the spatial  
11 correlations are considered more as a tool to regularize the inverse problem, rather than an  
12 uncertainty feature. Schuh et al. (2010) obtained correlation lengths from Rödenbeck et al.  
13 (2003) but with a much higher state space resolution of 200 km. Lauvaux et al. (2008) neglected  
14 the spatial correlations to enlarge the impact of the data. Carouge et al. (2010a) inferred spatial  
15 and temporal correlation lengths based on the agreement between posterior and “true” fluxes in  
16 the framework of a synthetic experiment, where the “truth” is known. A different approach was  
17 used in Peters et al. (2007) study where they interpret the length scale from a climatological and  
18 ecological perspective, and use it to spread information within regions, which the network is  
19 incapable to constrain. Ad-hoc solutions have also been used, assuming that daily fluxes have  
20 smaller correlation lengths than monthly fluxes which are used by other studies (Peylin et al.  
21 2005). More specifically Peylin et al. (2005) assumed 500 km for daily temporal resolution  
22 compared to the much larger correlation lengths used by Rödenbeck for monthly flux resolution.  
23 Michalak et al. (2004) implemented a geostatistical approach to describe the prior error structure.  
24 Specifically the prior error covariance describes at which degree deviations of the surface fluxes  
25 from their mean behavior at two different locations or times are expected to be correlated as a  
26 function of the distance in space or in time. They simultaneously estimate posterior fluxes as  
27 well as parameters controlling the model-data mismatch uncertainty and the prior flux  
28 uncertainty, including spatial and temporal correlation lengths. Although this approach may be  
29 considered as an objective way to infer spatial and temporal correlation lengths, it forces the  
30 error covariance to be statistically consistent with the atmospheric data from the few regions  
31 where station-to-station distances are small enough to be comparable to the correlation length



1 scales. Eddy Covariance stations (EC) can provide a more direct method to infer spatial and  
2 temporal flux correlations. Chevallier et al. (2006) and Chevallier et al. (2012) introduced  
3 autocorrelation analysis of the residual between fluxes simulated by biosphere models or  
4 measured by EC to infer spatial and temporal error correlations. The derived error statistics were  
5 implemented in a regional CO<sub>2</sub> inversion by Broquet et al. (2013).

6 Daily NEE flux residuals from model - data comparisons showed temporal correlations up to 30  
7 days but very short spatial correlations up to 40 km (Kountouris et al. 2015). In such a case the a-  
8 priori integrated uncertainty over time and space, e.g. annually and EU wide domain integrated,  
9 according to the error propagation will be exceptionally small. For example a variance of 1.82  
10  $\mu\text{mole.m}^{-2}.\text{s}^{-1}$  (from model – data differences) combined with the abovementioned correlation  
11 scales yields an uncertainty of 0.12 GtC y<sup>-1</sup> for the total flux over Europe. This value is  
12 significantly smaller than the assumed uncertainty which is typically used by the inversion  
13 systems. For comparison we refer to studies from Rivier et al. (2010) and Peylin et al. (2005) (for  
14 a slightly larger domain than ours) where an a priori uncertainty of approximately 1.4 GtC y<sup>-1</sup>  
15 and 1 GtC y<sup>-1</sup> respectively was used. Further, Peylin et al. (2013) found that the variance of the  
16 posterior NEE fluxes for the European domain among 11 global inversions is also 3 to 4 times  
17 larger (0.45 GtC y<sup>-1</sup>). Although is not yet entirely clear what would be the “correct” value for the  
18 prior uncertainty, it seems that in our study it should be increased not only to give enough  
19 flexibility to the system to adjust but also to be at least comparable with other posterior  
20 uncertainty estimates. A typical method is to inflate the spatiotemporal component by scaling  
21 accordingly the prior error covariance. In a study by Lauvaux et al. (2012) two correlation  
22 lengths were used at 300 and 50 km, and for the shorter scale the uncertainty was inflated by  
23 increasing the RMS of the prior error covariance. The model - data analysis (Kountouris et al.  
24 2015) does neither justify the use of large correlation scales nor largely inflated variances which  
25 exceed the model-data flux mismatches, however it is consistent with an additional overall bias  
26 error which can not be captured from the estimated spatiotemporal error structure. Hence an  
27 appropriate approach would be to introduce two adjustable terms into the inversion system. One  
28 term to reflect the data-derived error structure without error inflation (prior error covariance  
29 matrix which describes the spatiotemporal component) and one term to represent a bias  
30 component. To the best of our knowledge such an approach has not yet been used in inversion  
31 systems.



1 This study primarily aims to use the information extracted from the model-EC data residuals  
2 (spatiotemporal error structure) to define a data-driven error covariance rather than simply  
3 assuming one, adopting a conservative one or an expert knowledge solution. For that, we  
4 implement our previous methodology and findings regarding the prior uncertainty to atmospheric  
5 inversions following Kountouris et al. (2015). As explained above, we implement two  
6 uncertainty terms; the first one to reflect the true spatiotemporal error structure and the second  
7 term referred to a bias term. We use the Jena inversion system (Rödenbeck, 2005; Rödenbeck et  
8 al., 2009) for the regional scale consisting of a fully coupled system as described in Trusilova et  
9 al. (2010), between the global three-dimensional atmospheric tracer transport model TM3  
10 (Heimann and Körner, 2003) and the regional stochastic Lagrangian transport model STILT (Lin  
11 et al., 2003). This scheme allows retrieving surface fluxes at much finer resolution ( $0.25^\circ$ )  
12 compared to global models. The first part of this study details the methodology of the prior error  
13 implementation, and evaluates the system's performance through a synthetic data experiment.  
14 The system evaluation is an extension of Trusilova et al. (2010) where the evaluation was limited  
15 to the observation space only. We extend that to the flux space by comparing flux retrievals at  
16 various spatial and temporal scales against synthetic "true" fluxes. Station locations and  
17 observation times (including gaps) were created as in the real observation time series presented  
18 in the second part of this study (Kountouris et al., 2016). That way we can use the synthetic  
19 experiment to evaluate to what extent we can trust the results, if a real-data inversion is  
20 performed. In the second part of this study (Kountouris et al., 2016) the regional inversion  
21 system is applied to real observations of atmospheric  $\text{CO}_2$  mole fractions from a network of 16  
22 stations.

23 This paper is structured as follows. In Section 2 we present the inversion scheme and introduce  
24 the settings of the atmospheric inversions. In Section 3 we present the results from a synthetic  
25 inversion experiment aimed to assess the prior error setup, considering it as a step towards  
26 atmospheric inversions using real atmospheric data with an objective, state of the art prior error  
27 formulation. Discussion and conclusions are following in Section 4.

28



## 1    2 Methods

### 3    2.1 Inversion scheme

4  
 5    The Jena Inversion System (Rödenbeck 2005; Rödenbeck et al., 2009) was used for the current  
 6    study. The scheme is based on the Bayesian inference and uses two transport models, the TM3  
 7    model (Heimann and Körner, 2003) for global, and the STILT model (Lin et al., 2003) for  
 8    regional simulations. The advantage of the system is that it combines a global transport model  
 9    with a regional one without the need of a direct coupling along the boundaries. The global is  
 10    used to calculate fluxes from the far field (outside of the regional domain of interest), and  
 11    subsequently this information can be used to provide lateral boundary information for the  
 12    regional model. Primary input of the system is the observed mixing ratios  $c_{meas}$ . This vector  
 13    contains all measured mixing ratios at different times and locations. The modeled mixing ratios  
 14     $c_{mod}$  given from a temporally and spatially varying discretized flux field  $f$  are computed from an  
 15    atmospheric transport model and can be formally expressed as

$$16 \quad c_{mod} = Af + c_{ini} \quad (1)$$

17    where  $c_{ini}$  is the initial concentration and  $A$  the transport matrix which maps the flux space to the  
 18    observation space. For the regional domain the transport matrix  $A$  has been pre-computed by the  
 19    STILT transport model. The system calculates the modeled concentrations when and where a  
 20    measurement exists in the  $c_{meas}$  vector.

21    In the following, we briefly describe the inverse modeling approach. For more details the reader  
 22    is referred to Rödenbeck (2005).

23    In grid-based atmospheric inversions the number of unknowns (spatially and temporally resolved  
 24    fluxes) is larger than the number of measurements (hourly dry mole fractions at different sites),  
 25    making the inverse problem ill-posed. In the Bayesian concept this can be remedied by adding a-  
 26    priori information. This information can be written as

$$27 \quad f = f_{fix} + F \cdot p \quad (2)$$





1 where  $f_{fix}$  is the a-priori expectation value of the flux, matrix  $F$  contains all the a-priori  
 2 information about flux uncertainties and correlations (implicitly defining the covariance matrix)  
 3 and  $p$  is a vector representing the adjustable parameters. The parameters  $p$  are uncorrelated with  
 4 zero mean and unit variance. This flux model represents just a different way to define the a-priori  
 5 probability distribution of the fluxes, than the traditional way where the a-priori error covariance  
 6 matrix is explicitly specified. The cost function describing the observational constrain is  
 7 expressed as

$$8 \quad J_c = \frac{1}{2} (c_{meas} - c_{mod})^T \cdot Q_c^{-1} \cdot (c_{meas} - c_{mod}) \quad (3)$$

9 where  $Q_c$  is the observation error covariance matrix. This diagonal matrix weights the mixing  
 10 ratio values considering measurement uncertainty, location-dependent model uncertainty and a  
 11 data density weighting. The latter ensures that the higher amount of data from continuous  
 12 measurements compared to the data from flask measurements would not lead to a considerably  
 13 stronger impact of these corresponding sites (Rödenbeck, 2005). This can also be formally  
 14 interpreted as a temporal correlation scale which ensures that the model-data-mismatch error is  
 15 not independent within a week, corresponding roughly to time scales of synoptic weather  
 16 patterns.

17 The inversion system seeks to minimize the following cost function that combines the  
 18 observational (Eq. 3) and the prior flux constrain

$$19 \quad J = J_c + \frac{1}{2} \cdot p^T \cdot p \quad (4)$$

20 The minimization of the cost function is done iteratively with respect to the parameters  $p$  by  
 21 using a Conjugate Gradient algorithm with re-orthogonalization (Rödenbeck 2005).

22

23

24



## 2.2 Characteristics of the inversion set up

### 2.2.1 A-priori information and uncertainties

The a-priori CO<sub>2</sub> flux fields were derived from the Vegetation Photosynthesis and Respiration Model, VPRM (Mahadevan et al., 2008). VPRM uses ECMWF operational meteorological data for radiation (downward shortwave radiative flux) and temperatures (T2m), the SYNMAP landcover classification (Jung et al., 2006), and EVI (enhanced vegetation index) and LSWI (land surface water index) derived from MODIS (Moderate Resolution Imaging Spectroradiometer). Model parameters were re-optimized for Europe using eddy covariance measurements made during 2007 from 47 sites (a full site list is given in Kountouris et al. (2015); we excluded some sites due to insufficient temporal data coverage or lack of representativeness). To mediate the impact of data gaps, a data density weighting was introduced that takes into account the coverage of different times of the day (using 3-hour bins) in the different seasons. Optimized parameters are shown in Table 1. The net ecosystem exchange at hourly scale and at 0.25° x 0.25° spatial resolution for 2007 was simulated with the optimized parameters for the European domain shown in Fig. 1. The domain-wide aggregated biospheric carbon budget for 2007 derived that way from VPRM was found to be -0.96 GtC y<sup>-1</sup> (i.e. uptake by the biosphere). Note that without the density weighting an even stronger flux of -1.35 GtC y<sup>-1</sup> was derived, indicating the importance of proper treatment of data gaps by either gap-filling or by the inclusion of weights.

Additionally, biogenic CO<sub>2</sub> fluxes were simulated with the BIOME-BGC model, specifically its global implementation as GBIOME-BGCv1 (Trusilova and Churkina 2008) at the same 0.25° x 0.25° spatial and hourly temporal resolution. The purpose of the second flux field is to provide a perfectly known flux distribution as “true” fluxes that can be used to generate synthetic observations. The a-priori flux in a real-data inversion would have three components including fossil fuel and ocean fluxes

$$f_{pr} = f_{pr,nee} + f_{pr,ff} + f_{pr,oc} \quad (5)$$



1 We note that for the synthetic case the last two terms are set to zero. Similarly the deviation term  
 2 (the data-derived correction to the a-priori fluxes) of the flux model consists of the terms  
 3 referring to NEE, fossil fuel, and ocean fluxes but equivalently the last two terms are set to zero  
 4 for the synthetic inversion.

$$5 \quad F \delta s = (F_{nee}, F_{oc}, F_{ff}) \begin{pmatrix} \delta s_{nee} \\ \delta s_{oc} \\ \delta s_{ff} \end{pmatrix} \quad (6)$$

6 Note that the a-priori error covariance matrix does not explicitly appear in the inversion, but is  
 7 included though the second term in Eq. 8 (see section 2.2.2).

8 According to this formulation the columns of  $G_{tcor}$  and  $G_{xycor}$  contain the spatiotemporal extents  
 9 of the individual NEE pulses (range of values between 0 and 1) and the diagonal matrix  $f_{sh}(x,y,t)$   
 10 contains the pixel-wise a priori uncertainties. These uncertainties were chosen to be flat  
 11 (constant) in space and time. For more detailed information the reader is referred to Rödenbeck  
 12 et al. (2005).

13 The total prior uncertainty was chosen according to the mismatch between VPRM and BIOME-  
 14 BGCv1, calculated as the annual and domain wide integrated flux mismatch. Prior fluxes and the  
 15 fluxes representing the synthetic truth are strongly different ( $-0.96 \text{ GtC y}^{-1}$  and  $-0.31 \text{ GtC y}^{-1}$  for  
 16 VPRM and GBIOME-BGCv1, respectively). The error structure used for the synthetic study is  
 17 estimated according to the method applied in Kountouris et al. (2015). Time-series of daily  
 18 fluxes were extracted for both biosphere models at grid cell locations where an EC station exists.  
 19 Then spatial and temporal autocorrelation analysis was performed on the daily model-model flux  
 20 residuals, yielding a spatial correlation length scale of 566 km and a temporal correlation scale of  
 21 30 days.

22 The eddy covariance station locations used for this analysis were exactly the same as in  
 23 Kountouris et al. (2015) ensuring similarity in the derivation of the error structure for the  
 24 synthetic data inversions. However of note is that for the synthetic data inversions, prior fluxes  
 25 from VPRM model were not optimized against GBIOME-BGCv1 “true” fluxes.



1 The implicitly defined prior error covariance matrix contains diagonal elements of  $(1.45 \mu\text{mol m}^{-2} \text{ s}^{-1})^2$ , which reflect the variance from model-model flux mismatches at the 50 km spatial  
 2 resolution of the state space. Exponentially decaying spatial correlations were implemented with  
 3 a correlation scale of 766 km at the zonal and 411 km at the meridional direction, roughly  
 4 corresponding to the 566 km correlation scale yielded from the model-model residual  
 5 autocorrelation analysis and preserving the same zonal/meridional ratio as in the global  
 6 inversion. Temporal autocorrelation was set to 31 days, which is consistent with the Kountouris  
 7 et al. (2015) analysis. These scales result in an uncertainty for the spatiotemporal component  
 8 ( $E_{st}$ ) domain-wide and annually integrated of  $0.44 \text{ GtC y}^{-1}$ . We chose two different approaches to  
 9 increase the prior uncertainty at domain-wide and annually integrated scale such that it matches  
 10 the mismatch of  $0.65 \text{ GtC y}^{-1}$  between the two biosphere models. First we inflate the error by  
 11 scaling the error covariance matrix, this case is referred to as base case B1 hereafter. The second  
 12 approach, referred to as scenario S1, could be considered as a more formal way: we introduce an  
 13 additional degree of freedom to the inversion system by allowing for a bias term. This term is  
 14 spatially distributed according to the annually averaged VPRM respiration component, and is  
 15 kept constant in time. The error  $E_{BT}$  of the bias component was adjusted such that the total prior  
 16 error  $E_{tot}$  for annually and domain-wide integrated fluxes matches the targeted total uncertainty:  
 17

$$18 \quad E_{tot}^2 = E_{st}^2 + E_{BT}^2 \quad (7)$$

19 This resulted in an overall uncertainty  $E_{tot}$  of  $0.65 \text{ GtC y}^{-1}$ , which is identical to the mismatch  
 20 between the two biosphere models.

21

22

### 23 2.2.2 State space

24

25 The inversion system optimizes additive corrections to three-hourly fluxes in a sense that the  
 26 posterior flux estimate can be given by the sum of a fixed a priori term (first term of the right  
 27 hand side in Eq. 8) and an adjustable term (second term in Eq. 8). The latter has a-priori a zero  
 28 mean and unit variance. The biogenic fluxes can be defined as follows:



$$f(x, y, t) = f_{fix}(x, y, t) + f_{sh}(x, y, t) \cdot \sum_{m_t}^{N_t} \sum_{m_s}^{N_s} G_{icor, m_t}(t) \cdot G_{xycor, m_s}(x, y) \cdot p_{inv, m_t, m_s} \quad (8)$$

where  $f_{sh}$  is a shape function which defines the adjustable term. The spatial and temporal correlation structures of the uncertainty are described by the pulse response functions  $G_{xycor}$  and  $G_{icor}$  respectively. The term  $p_{inv}$  contains the adjustable parameters which they a-priori have, a Gaussian distribution with zero mean and unit variance.

For the S1 case the posterior flux estimates can be derived by adding the optimized bias flux field to Eq. 8

$$f(x, y, t) = f_{fix}(x, y, t) + f_{sh}(x, y, t) \cdot \sum_{m_t}^{N_t} \sum_{m_s}^{N_s} G_{icor, m_t}(t) \cdot G_{xycor, m_s}(x, y) \cdot p_{inv, m_t, m_s} + f_{sh}^{BT}(x, y) \cdot \sum_{m_t}^{N_t} G_{icor, m_t}(t) \cdot p_{BT} \quad (9)$$

The bias term  $f_{sh}^{BT}$  follows a flux shape (here we used annually averaged respiration, with no temporal variation).

### 2.2.3 Observation vector and uncertainties

The observation vector  $c_{meas}$  contains mixing ratio observations at all site locations and sampling times. A common procedure to derive synthetic observations is to create a “true” flux field by adding some error realizations to the a-priori fluxes (Schuh et al., 2009; Broquet et al., 2011) or to perturb the resulting synthetic observations (Wu et al., 2011). For the current study instead we use a different biosphere model, the GBIOME-BGCv1 model, to derive biogenic CO<sub>2</sub> fluxes at hourly scale. Then a forward transport model run was performed to create synthetic mixing ratios at hourly resolution for each station location. This choice of using two different biosphere models for deriving the a-priori and the “true” fluxes is expected to increase the realism of the synthetic data study, given the fact that the real spatiotemporal flux distribution is highly unknown (though the model-to-model difference may not accurately reflect the model errors either). For the synthetic study, observations were created for the same station locations and



1 observation times as in the real observation time series which are used in the second part of this  
2 study (Kountouris et al., (2016)). An overview of the atmospheric stations is given in table 2.  
3 The data coverage per station is shown in Figure 2. Only daytime observations were considered  
4 (11:00 – 16:00 local time) since the transport model is expected to perform worse during night  
5 when a stable boundary layer forms. An exception is made for mountain stations that measure  
6 the free troposphere, where only nighttime observations (23:00 – 04:00 local time) were  
7 considered, as this time can be better represented by the transport model. In total 20273 hourly  
8 observations from the year 2007 were used.

9 The model-data mismatch uncertainty associated with each measurement is expressed as a  
10 diagonal covariance matrix, and contains measurement errors and errors from different  
11 components describing the modeling framework (i.e. model errors due to imperfect transport,  
12 aggregation errors, etc.) (Gerbig et al., 2003b). For the current study, all sites are classified  
13 according to their characteristics (e.g. tall tower, mountain sites etc.), and uncertainties were  
14 defined depending on the site class (Figure 2, legend on the right). The uncertainties are  
15 considered as representative for current inverse modeling systems. Although the measurement  
16 error covariance is a diagonal matrix, we do consider for temporal correlations via a data density  
17 weighting (see Section 2.1).

#### 19 **2.2.4 Atmospheric transport**

20

21 For the synthetic data study only the regional atmospheric model STILT was used to create the  
22 observations with a forward run, and to perform the inversion. This was feasible since the  
23 synthetic CO<sub>2</sub> observations are only influenced by fluxes occurring within the DoI, hence global  
24 runs to retrieve boundary conditions at the edge of DoI are not necessary. The transport matrix  
25 for the regional inversions was generated in form of pre-calculated footprints (sensitivities of  
26 atmospheric observations to upstream fluxes) at 0.25 degrees spatial and hourly temporal  
27 resolution for the full year 2007. STILT trajectory ensembles were driven by ECMWF  
28 meteorological fields (Trusilova et al., 2010), and computed for 10 days backwards in time,  
29 ensuring that nearly all trajectories have left the domain of interest.



## 2.3 Metrics for performance evaluation

Following Rödenbeck et al. (2003) we evaluate the goodness of fit for each station (station specific  $\chi^2$ ). The modeled dry mole fractions should be with 68% probability within the  $\pm 1\sigma$  range from the observed mole fractions. This is equivalent to the requirement that the dry mole fraction part of the cost function defined as the sum of hourly squared differences, divided by the uncertainty interval and the number of observations  $n$  (Eq. 10), should be close to unity.

$$\chi_c^2 = \frac{\sum_i \frac{(\Delta c_i)^2}{\sigma_i^2}}{n} \quad (10)$$

Another important aspect is the reduced  $\chi_r^2$  metric that compares the a-priori model performance with the specified error structure by dividing the squared residuals of optimized minus observed dry mole fractions by the squared specified uncertainties. This is also equivalent to two times the cost function at its minimum divided by the number of degrees of freedom (effective number of observations) (Thompson et al., 2011):

$$\chi_r^2 = 2 \frac{J_{\min}}{n} \quad (11)$$

Again, a correct balance should be close to unity. Smaller values suggest that the model performance was better than specified in the covariance structure and hence the assumed uncertainties (denominator) were conservative.

In flux space, we evaluate the inversion performance, by comparing the retrieved flux estimates against the synthetic fluxes (“true”) at different temporal and spatial scales: annually and monthly integrated fluxes, domain-wide and at country scale. In particular we are interested in capturing the “true” fluxes down to country scale. For that we assess monthly posterior retrievals which we compare to reference data (“true” fluxes), country aggregated, using a Taylor diagram. This diagram provides a concise statistical summary of how well patterns match each other in terms of their correlation and the ratio of their variances.



## 3 Results

The purpose of the synthetic study is to evaluate the system set-up with a realistic approach. To evaluate the ability of the system to retrieve the synthetic true fluxes we visualize spatially distributed fluxes and we study spatially integrated (domain and national scale) as well as temporally (annual and monthly scale) integrated fluxes.

### 3.1 CO<sub>2</sub> mole fractions

A comparison of true and modeled CO<sub>2</sub> dry mole fractions from forward runs of the optimized fluxes can reveal the goodness of fit, realized through the optimization process. Such a comparison is presented in Figure 3 for the Schauinsland (SCH) continuous station. Both B1 and S1 inversions significantly reduce the misfit between the synthetic (truth) and the a-priori mole fractions. The RMSD between the prior/posterior from the “true” timeseries for all stations (Table 3) shows an average reduction of around 74% and 76% for the S1 and B1 inversions respectively. Prior correlations (prior vs. true dry mole fractions), have an averaged value of 0.46 which is increased to 0.93 for both inversions. Significant differences between the two inversions were not found apart from a slightly larger decrease of the RMSD for the B1 case. Figure 4 summarizes the capability of the inversions to capture the true signal at each station location in form of a Taylor diagram, indicating that the inversions showed a significant increase of the correlation for all sites. Further the variance of the modeled time-series is significantly closer to the variance of the true signal.

To estimate the goodness of fit we consider the station specific  $\chi_c^2$  values (Eq. 10), using here 7-day aggregated residuals instead of hourly to match the temporal scale of one week of the observation error. Values smaller than 1 are found for most of the stations with a mean value of 0.28 and 0.32 for the B1 and S1 cases respectively, suggesting a good fitting performance for all stations and for both inversions. The results are comparable with those found in the Rödenbeck et al. (2003) study. The reduced chi-squared (Eq. 11) was found to be 0.21 for both cases, indicating that the error variance is overestimated making the error assumption rather conservative.





### 3.2 Flux estimates and uncertainties

The spatial distributions of the annual biosphere-atmosphere exchange fluxes for the prior, the known truth, and the posterior cases are presented in Figure 5. Note that annual fluxes between the two biosphere models used for prior fluxes and true fluxes are substantially different. The inversion significantly adjusts the spatial flux distribution mainly in central Europe, where a denser atmospheric network exists. The absolute annual mean difference in fluxes ( $|\text{mean}(\text{true} - \text{prior})|$  and  $|\text{mean}(\text{true} - \text{posterior})|$ ) is greatly reduced from  $70.8 \text{ gCm}^{-2}\text{y}^{-1}$  to  $14.7 \text{ gCm}^{-2}\text{y}^{-1}$  and  $24.6 \text{ gCm}^{-2}\text{y}^{-1}$  for the B1 and S1 inversions respectively. Detailed patterns, however, are not well reproduced: the fraction of explained spatial variance in the true fluxes (measures as squared Pearson correlation coefficient) decreases from the prior (0.17) to the posterior (0.07 and 0.06 for the cases B1 and S1, respectively). When evaluating this at monthly scales, the fraction of explained spatial variance increases in the posterior estimates compared to the prior for winter months from around 0-15% to about 15-50%, while during the growing season typically a decrease from around 10-35% to about 0-34% is found. The accumulated footprint of the atmospheric network is shown in Figure 6, clearly indicating the strongest constraint on fluxes in central Europe. Interestingly both error structures from S1 and B1 inversions produce posterior fluxes that have approximately the same spatial distribution. When separating the spatiotemporal component from the bias component (in S1 case) we can identify differences between the two inversions. Significant deviations of the spatial flux distribution between the spatiotemporal components were found: The spatiotemporal component in the S1 case has a domain wide annual flux correction of  $0.39 \text{ GtC y}^{-1}$  (prior – posterior) while the corresponding term in the B1 case has a correction of  $0.78 \text{ GtC y}^{-1}$ . Nevertheless standard deviations of the corrections with respect to the true spatial flux distribution (true – posterior) found to have no significant difference ( $6.88 \cdot 10^{-5}$  and  $7.38 \cdot 10^{-5} \text{ GtC y}^{-1}\text{cell}^{-1}$  for S1 and B1 respectively). We do not observe any strong correction in the south-eastern part of Europe as it cannot be “seen” from the atmospheric network due to the distance to the observing sites and the prevailing westerly winds. This could also be inferred from the flux innovation plots (see Figure 5) defined as the difference between prior and posterior fluxes. Only very small or even no corrections occurred in this area.

We are specifically interested in the ability of the inversion system to capture integrated fluxes over time and space. Figure 7 shows an overview of the domain-integrated fluxes at a monthly



1 and annual scale. Despite the remarkably larger a-priori (VPRM) sink compared to the synthetic  
2 truth (GBIOME-BGCv1) during the growing season, both inversions, with and without the bias  
3 term, produce posterior flux estimates that fully capture the "true" monthly and annually  
4 integrated fluxes. While the monthly posterior estimates give no clear evidence on which  
5 inversion performs better, retrievals at annual scale slightly favor the inversion without the bias  
6 term (B1 case). A difference was observed in the prior uncertainties between the two inversions.  
7 While both were scaled to have the same prior annual uncertainty, the B1 inversion has  
8 systematically larger prior monthly uncertainties than the S1 as a result of the inflated  
9 spatiotemporal component of the prior error covariance. Posterior uncertainties were found to be  
10 similar, and include or are close to including (S1 case) the true flux estimates. The uncertainty  
11 reduction for annually and domain-wide integrated fluxes, defined as the difference between  
12 prior and posterior uncertainties normalized by the prior uncertainty, was found to be 73% and  
13 69% for the S1 and B1 respectively.

14 In order to assess how well the posterior estimates agree with the true fluxes, root mean square  
15 difference (RMSD) between true and posterior monthly integrated gridded fluxes were computed  
16 (Table 4). Both inversions B1 and S1 show a similar reduction in the RMSD values compared to  
17 the prior. The same picture emerges for the annually integrated fluxes.

18 Of particular interest is the performance of the system at regional scale, specifically at national  
19 level. Figure 8 shows monthly fluxes for selected European countries, including the prior, true  
20 and posterior estimates with the corresponding uncertainties. Both error structures show a similar  
21 performance. Despite the large prior misfit, the system succeeded in retrieving monthly fluxes at  
22 country level. Better constrained regions mainly located in central Europe show the ability to  
23 broadly capture the temporal flux variation at monthly scale. Figure 9 summarizes in a Taylor  
24 diagram the inversion performance for each EU-27 country, showing the improvement of  
25 monthly and country aggregated fluxes (perfect match would be if the head of the arrow  
26 coincides with the reference point marked as green bullet). It is worth mentioning that also for  
27 regions that are less constrained by the network, such as Great Britain, Spain, Poland and  
28 Romania, the inversions still improved the posterior estimates compared to the prior estimates  
29 (see also Fig. 9).

30



### 3.3 Evaluation with synthetic eddy covariance data

In order to investigate the potential of using eddy covariance measurements for evaluating the retrieved CO<sub>2</sub> fluxes, monthly fluxes from the prior (VPRM), the truth (GBIOME-BGCv1), and the posterior for cases B1 and S1 were extracted at the grid cell locations where eddy covariance stations exist, using the same 53 sites as in Kountouris et al. (2015). The corresponding fluxes were then aggregated over all sites, using a weight that compensates for the asymmetry between number of flux towers for specific vegetation types and the fraction of land area covered by the specific vegetation type. Prior fluxes show a systematically larger uptake compared to the truth, predominantly during the growing season with maximum differences of 0.8 gCm<sup>2</sup>day<sup>-1</sup> (Figure 10). Posterior estimates for both cases captured the magnitude of the true fluxes, with maximum differences of around 0.3 gCm<sup>2</sup>day<sup>-1</sup> during June/July. A significantly larger correction is apparent during spring and summer compared to winter and fall. The very close correspondence of these results with those shown in Figure 7 for the domain-wide monthly flux budget clearly shows that eddy covariance measurements can principally be used for validation of the inverse estimates at monthly timescales.

## 4 Discussion

### 4.1 Performance in flux space

Results from the synthetic experiment showed the strengths but also the weaknesses of the system to retrieve the “true” spatial flux distribution. Although the error structure applied to this experiment was statistically coherent with the mismatch between prior and true fluxes, we note a limited ability of the current atmospheric network to retrieve fluxes at local scales. For coarser spatial scales (country level) the carbon budget estimates in the synthetic inversion showed a quite good performance at monthly and annual temporal scales. Further we observed an average reduction of the monthly uncertainties of 65% for the B1 case, and 64% for the S1 case. In



1 combination with the fact that the flux estimates reproduce the “truth” within the posterior  
2 uncertainties, this gives us confidence in the accuracy of our estimates.

3 Prior error correlation in time and space limits the scale, at which information can be retrieved  
4 from the inversion. The spatial correlation of several hundred kilometers implies that fluxes at  
5 scales smaller than this cannot be significantly improved by the inversion, as the results clearly  
6 showed. To assess this more quantitatively, the spatial correlation between a priori or retrieved  
7 and true monthly fluxes is calculated for different spatial aggregation scales (starting at 0.25  
8 degree, fluxes were aggregated to 0.5, and then in 1-degree steps up to 8 degree). Results shown  
9 in Fig. 11 a) indicate a nearly continuous increase of the spatial correlation of prior and posterior  
10 fluxes with increasing aggregation scale. The additional explained variance brought about by the  
11 inversion, i.e. the difference between posterior (red/blue line) and prior (grey line) flux  
12 correlation (r-square) with the truth, starts at low values around 0.1, and reaches values around  
13 0.2 for scales larger or equal 2 degrees. Similarly, the spatial correlation between a priori and  
14 true fluxes for a given spatial aggregation of 2 degrees, but for different temporal aggregation  
15 scales ranging from 1 day to 128 days (Fig. 11 b) shows a continuous increase from about 0.23 to  
16 0.42 (r-square), while the spatial correlation between retrieved and true fluxes only varies  
17 slightly between 0.4 and 0.53 (Fig. 11 b), red and blue lines). Here, the additional spatial  
18 variance explained by the retrieved fluxes is largest at around monthly time scales (differences  
19 between prior and posterior r-square around 0.2), while at seasonal scales this additional  
20 explained variance is only around 0.1. Overall, this analysis confirms that there are preferred  
21 spatial and temporal scales at which the inversion retrieves the flux distribution best and where  
22 thus most information is gained. This is not dependent on whether or not a bias term is included  
23 in the state vector, as results for case B1 and S1 do not differ in this regard. It is important to  
24 realize that all other scales, at which the inversion does not provide much information, need to be  
25 properly represented by the a priori flux distribution. Thus the a priori fluxes need to be realistic  
26 at short spatial scales below about 200 km, at seasonal temporal scales, and of course at hourly  
27 time scales which are not retrieved by the inversion.

28 The annual spatial flux distribution of the B1 and S1 cases was found to be quite similar,  
29 indicating that inflating the uncertainty by a factor of 1.5 (B1 case, see also 2.2.1 section) or  
30 adding a bias component to compensate the inflation (S1 case) lead to a similar flux constraint.



1 This could be explained due to the long correlation length (566 km) which drastically reduces the  
2 effective number of degrees of freedom, forcing the fluxes to be smoothly corrected, regardless  
3 the use of the bias component.

4

## 5 **4.2 Performance in observation space**

6

7 The high RMSD reduction in combination with the high correlation values and the captured  
8 variability between posterior and true dry mole fractions in the synthetic experiment suggest a  
9 good performance of the inversion system to retrieve the “true” mixing ratios. Nevertheless this  
10 is not surprising, as the atmospheric data are “fitted” by the inversion, and furthermore the  
11 forward and the inverse runs used identical transport, without any impact from imperfections in  
12 transport simulations.

13 The uncertainties in the flux space are statistically consistent with the model-model flux  
14 mismatch. However the reduced  $\chi_r^2$  values obtained from the inversions were rather small  
15 (around 0.21). This indicates that overall conservative uncertainties were assumed, and the small  
16  $\chi_r^2$  values are a result from the assumed uncertainties in the observation space. Indeed  
17 uncertainties in the observation space include also transport uncertainties; however, given that  
18 the same transport is used to create synthetic observations and to perform the inversion, there is  
19 no actual model-data mismatch related to transport uncertainties, and so the assumed  
20 uncertainties are overestimated.

21

## 22 **5 Conclusions**

23

24 This paper describes the setup and the implementation of prior uncertainties as derived from  
25 model-eddy covariance data comparisons into an atmospheric CO<sub>2</sub> inversion. The inversion  
26 system assimilates hourly dry air mole fractions from 16 ground stations to optimize 3-hourly  
27 NEE fluxes for the study year 2007. Two different error structures were introduced to describe  
28 the prior uncertainty by either inflating the error or by adding an additional degree of freedom



allowing for a long term bias. The need of this error inflation comes from the fact that the spatiotemporal model - data error structure alone underestimates prior uncertainties typically assumed for inversion systems at continental/annual scale. In this study we evaluate the Jena inversion system by performing a synthetic experiment and expanding the evaluation also to the retrieved fluxes, whilst only the observation space was evaluated in Trusilova et al. (2010). Further we assess the impact when adding a bias term in the flux error structure. This study is a preparatory step to retrieving European biogenic fluxes using a data driven error structure consistent with model-flux data mismatches, which is described in the companion paper (Kountouris et al. 2016).

Significant flux corrections and error reductions were found for larger aggregated regions (i.e. domain-wide and countries), giving us confidence on the reliability of the results for a real data inversion. We found a similar performance for both error structures. A more detailed analysis of the spatial and temporal scales, at which the inversion provides a significant gain in information on the distribution of fluxes, clearly confirms that a) fluxes at spatial scales much smaller than the spatial correlation length used for the a priori uncertainty cannot be retrieved; b) the inversion performs best at temporal scales around monthly, and c) especially the small spatial scales need to be realistically represented in the a priori fluxes.

## Acknowledgments

This work contributed to the European Community's Seventh Framework Program (FP7) project ICOS-INWIRE, funded under grant agreement no. 313169. The authors would also like to thank the Deutsches Klimarechenzentrum (DKRZ) for using the high performance computing facilities. This publication is an outcome of the International Space Science Institute (ISSI) Working Group on "Carbon Cycle Data Assimilation: How to consistently assimilate multiple data streams" publication is an outcome of the International Space Science Institute (ISSI) Working Group on "Carbon Cycle Data Assimilation: How to consistently assimilate multiple data streams."



## Appendix

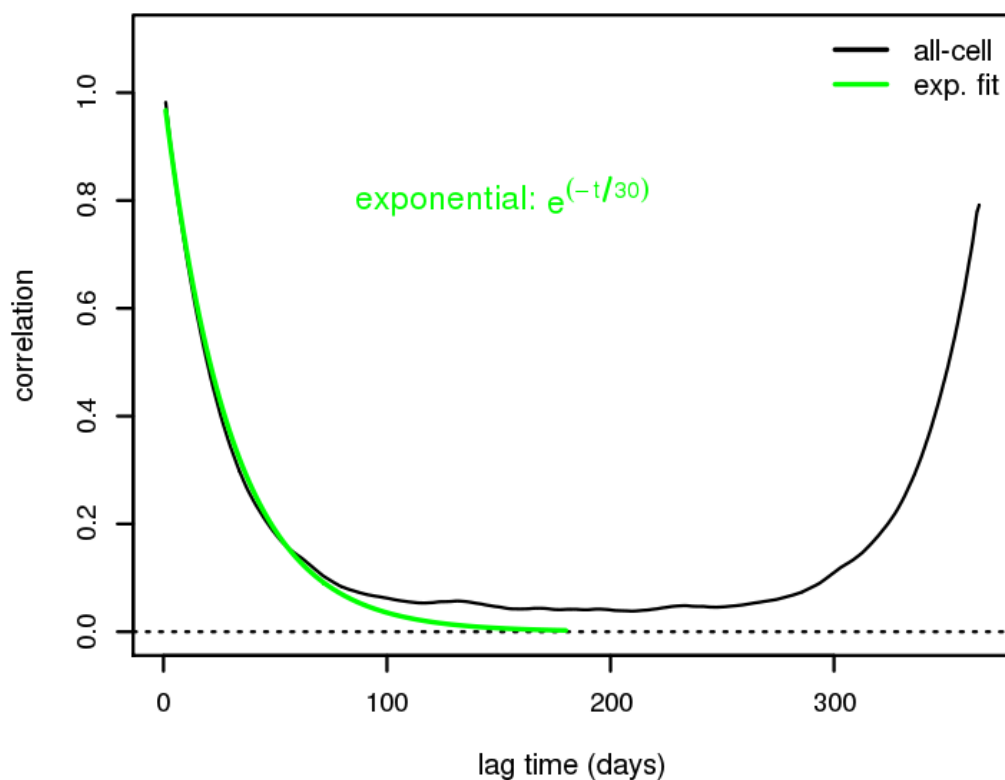
The exponentially decaying temporal autocorrelations is a feature newly implemented into the Jena Inversion System. Temporal correlations are not directly defined as off-diagonal elements in the a-priori error covariance, as the latter does not appear explicitly in the inversion. Rather, the inversion system involves time series filtering in terms of weighted Fourier expansions. More specifically the columns of matrix  $G_{\text{cor}}$  contain Fourier modes, weighted according to the frequency spectrum that corresponds to the desired autocorrelation function. The reader is referred to Rödenbeck (2005) for more information. Following Rödenbeck (2005) we define the following spectral weight  $w$ :

$$w = \frac{\nu_{\text{low}}}{\sqrt{\nu_{\text{low}}^2 + (2\pi\nu)^2}} \quad \text{A1}$$

where  $\nu_{\text{low}}$  is the characteristic frequency. The characteristic frequency  $\nu_{\text{low}}$  can be calculated from the desired temporal autocorrelation time (30 days) of the exponential decay and is expressed in years:

$\nu_{\text{low}} = 1/(1/12)$  where 1/12 is the autocorrelation time in years. Hence the characteristic frequency corresponding to a monthly autocorrelation is 12.

To test numerically whether the implemented autocorrelation decay shape approximates an exponential decay, an error realization of the characteristic frequency was added to the prior fluxes, and the autocorrelation function as described in Kountouris et al. (2015) was calculated numerically simultaneously for the flux time series of all grid cells. Then an exponentially decaying function was fitted (Fig. A1) to derive the autocorrelation scale for the corresponding frequency. The resulting autocorrelation shape indeed approximates very well an exponential decay, with an e-folding time of precisely 30 days. The tight confidence bounds of the fitted parameter (29.3 and 30.6 days within 95 % confidence interval), in combination with the small residual sum-of-squares (0.14) suggests a very good approximation of the exponential decay.



1

2 Figure A1: Autocorrelation function for a characteristic frequency of the exponential filter. The  
 3 autocorrelation is calculated simultaneously for all the domain grid cells. The numerical  
 4 realization of the autocorrelation does not decay to zero because of the flux seasonality.

5

6

7

8

9





1

2

### 3 **References**

4 Broquet, G., Chevallier, F., Bréon, F. M., Kadygrov, N., Alemanno, M., Apadula, F., Hammer,  
5 S., Haszpra, L., Meinhardt, F., Morguá, J. A., Necki, J., Piacentino, S., Ramonet, M., Schmidt,  
6 M., Thompson, R. L., Vermeulen, A. T., Yver, C., and Ciais, P.: Regional inversion of CO<sub>2</sub>  
7 ecosystem fluxes from atmospheric measurements: reliability of the uncertainty estimates,  
8 Atmos. Chem. Phys., 13, 9039-9056, doi:10.5194/acp-13-9039-2013, 2013.

9 Broquet, G., Chevallier, F., Rayner, P., Aulagnier, C., Pison, I., Ramonet, M., Schmidt, M.,  
10 Vermeulen, A. T. and Ciais, P.: A European summertime CO<sub>2</sub> biogenic flux inversion at  
11 mesoscale from continuous in situ mixing ratio measurements, J Geophys. Res., 116, D23303,  
12 doi:10.1029/2011JD016202, 2011.

13 Carouge, C., Bousquet, P., Peylin, P., Rayner, P. J., and Ciais, P.: What can we learn from  
14 European continuous atmospheric CO<sub>2</sub> measurements to quantify regional fluxes – Part 1:  
15 Potential of the 2001 network, Atmos. Chem. Phys., 10, 3107-3117, doi:10.5194/acp-10-3107-  
16 2010, 2010a.

17 Carouge, C., Peylin, P., Rayner, P. J., Bousquet, P., Chevallier, F., and Ciais, P.: What can we  
18 learn from European continuous atmospheric CO<sub>2</sub> measurements to quantify regional fluxes –  
19 Part 2: Sensitivity of flux accuracy to inverse setup, Atmos. Chem. Phys., 10, 3119-3129,  
20 doi:10.5194/acp-10-3119-2010, 2010b.

21 Chevallier F., Viovy N., Reichstein M. and Ciais, P.: On the assignment of prior errors in  
22 Bayesian inversions of CO<sub>2</sub> surface fluxes, Geophys. Res. Lett., 33, L13802, doi:  
23 10.1029/2006GL026496, 2006.

24 Chevallier, F., Wang T., Ciais P., Maignan F., Bocquet M., Altaf A. M., Cescatti A., Chen J.,  
25 Dolman A., J., Law B. E., Margolis, H. A., Montagnani, L., Moors, E. J.: What eddy-covariance  
26 measurements tell us about prior land flux errors in CO<sub>2</sub> flux inversion schemes, Glob.  
27 Biogeochem. Cy., 26, GB1021, doi:10.1029/2010GB003974, 2012.



- 1 Ciais, P., Peylin, P. and Bousquet, P.: Regional biospheric carbon fluxes as inferred from  
2 atmospheric CO<sub>2</sub> measurements, *Ecol Appl*, 10, 1574-1589, doi: 10.2307/2641225, 2000.
- 3 Ciais, P., Borges, A. V., Abril, G., Meybeck, M., Folberth, G., Hausglustaine, D., and Janssens,  
4 I. A.: The impact of lateral carbon fluxes on the European carbon balance, *Biogeosciences*, 5,  
5 1259-1271, doi: 10.5194/bg-5-1259-2008, 2008.
- 6 Ciais, P., Paris, J. D., Marland, G., Peylin, P., Piao, S. L., Levins, I., Pregar, T., Scholz, Y.,  
7 Friedrich, R., Rivier, L., Houwelling, S., Schuldze, E. D., and members of the CARBOEUROPE  
8 SYNTHESIS TEAM: The European carbon balance. Part1: fossil fuel emissions, *Glob Change*  
9 *Biol*, 16, 1395-1408, doi: 10.1111/j.1365-2486.2009.02098.x, 2009.
- 10 Dee, D. P., Uppala, S. M., Simmons, A. J., Berrisford, P., Poli, P., Kobayashi, S., Andrae, U.,  
11 Balmaseda, M. A., Balsamo, G., Bauer, P., Bechtold, P., Beljaars, A. C. M., van de Berg, L.,  
12 Bidlot, J., Bormann, N., Delsol, C., Dragani, R., Fuentes, M., Geer, A. J., Haimberger, L., Healy,  
13 S. B., Hersbach, H., Hólm, E. V., Isaksen, L., Kållberg, P., Köhler, M., Matricardi, M., McNally,  
14 A. P., Monge-Sanz, B. M., Morcrette, J.-J., Park, B.-K., Peubey, C., de Rosnay, P., Tavolato, C.,  
15 Thépaut, J. N. and Vitart, F.: The ERA-Interim reanalysis: configuration and performance of the  
16 data assimilation system. *Q.J.R. Meteorol. Soc.*, 137: 553–597. doi: 10.1002/qj.828, 2011.
- 17 Enting, I. G., Trudinger, C. M., and Francey, R. J.: A synthesis inversion of the concentration  
18 and  $\delta^{13}\text{C}$  of atmospheric CO<sub>2</sub>, *Tellus*, ser.B, 47, 35-52, 1995. Ferrarese S., Apadula F., Bertiglia  
19 F., Cassardo C., Ferrero A., Fialdini L., Francone C., Heltai D., Lanza A., Longhetto A., Manfrin  
20 M., Richiardone R., Vannini C.: Inspection of high-concentration CO<sub>2</sub> events at the Plateau  
21 Rosa Alpine station, *Atmospheric Pollution Research* 6, 415-427, doi:10.5094/APR.2015.046,  
22 2015.
- 23 Fiedler, V., Dal Maso, M., Boy, M., Aufmhoff, H., Hoffmann, J., Schuck, T., Birmili, W.,  
24 Hanke, M., Uecker, J., Arnold, F., and Kulmala, M.: The contribution of sulphuric acid to  
25 atmospheric particle formation and growth: a comparison between boundary layers in Northern  
26 and Central Europe, *Atmos. Chem. Phys.*, 5, 1773-1785, doi:10.5194/acp-5-1773-2005, 2005.
- 27 Gerbig, C., Lin, J. C., Wofsy, S. C., Daube, B. C., Andrews, A. E., Stephens, B. B., Bakwin, P.  
28 S. and Grainger, C. A.: Toward constraining regional-scale fluxes of CO<sub>2</sub> with atmospheric



- 1 observations over a continent: 1. Observed spatial variability from airborne platforms , J
- 2 Geophys Res – Atmos, 108, 4756, doi: 10.1029/2002JD003018, 2003a.
- 3 Gerbig, C., Lin, J. C., Wofsy, S. C., Daube, B. C., Andrews, A. E., Stephens, B. B., Bakwin, P.
- 4 S. and Grainger, C. A.: Toward constraining regional-scale fluxes of CO<sub>2</sub> with atmospheric
- 5 observations over a continent: 2. Analysis of COBRA data using a receptor-oriented framework ,
- 6 J Geophys Res, 108, 4757, doi: 10.1029/2003JD003770, 2003b.
- 7 Gerbig, C., Körner, S. and Lin, J. C.: Vertical mixing in atmospheric tracer transport models:
- 8 error characterization and propagation, Atmos. Chem. Phys., 8, 591-602, doi:10.5194/acp-8-591-
- 9 2008, 2008.
- 10 Gurney, K. R., Law, R. M., Denning, A. S., Rayner, P. J., Baker, D., Bousquet, P., Bruhwiler, L.,
- 11 Chen, Y.-H., Ciais, P., Fan, S., Fung, I. Y., Gloor, M., Heimann, M., Higuchi, K., John, J.,
- 12 Kowalczyk, E., Maki, T., Maksyutov, S., Peylin, P., Prather, M., Pak, B. C., Sarmiento, J.,
- 13 Taguchi, S., Takahashi, T., and Yuen, C. W.: TransCom and CO<sub>2</sub> inversion intercomparison 1.
- 14 Annual and mean control results and sensitivity to transport and prior flux information, Tellus
- 15 55B , 555-579, doi: 10.1034/j.1600-0889.2003.00049.x, 2003.
- 16 Gurney, K. R., Rachel M. L., Denning, A. S., Rayner, P. J., Bernard C. P., Baker, D., Bousquet,
- 17 P., Bruhwiler, L., Chen, Y.-H., Ciais, Fung, I. Y., Heimann, M., John, J., Maki, T., Maksyutov,
- 18 S., Peylin, P., Prather, M. and Taguchi, S.: Transcom 3 inversion intercomparison: Model mean
- 19 results for the estimation of seasonal carbon sources and sinks, Global Biogeochem. Cy., 18,
- 20 GB1010, doi:10.1029/2003GB002111, 2004.
- 21 Heimann, M. and Körner, S.: The global atmospheric tracer model TM3, Tech. Rep. 5, MPI
- 22 BGC, Jena (Germany), online available at: [http://www.bgc-](http://www.bgc-jena.mpg.de/mpg/websiteBiogeochemie/Publikationen/Technical%20Reports/tech%20report5.pdf)
- 23 [jena.mpg.de/mpg/websiteBiogeochemie/Publikationen/Technical Reports/tech report5.pdf](http://www.bgc-jena.mpg.de/mpg/websiteBiogeochemie/Publikationen/Technical Reports/tech report5.pdf), 2003.
- 24 Houweling, S., Aben, I., Breon, F.-M., Chevallier, F., Deutscher, N., Engelen, R., Gerbig, C.,
- 25 Griffith, D., Hungershoefer, K., Macatangay, R., Marshall, J., Notholt, J., Peters, W., and Serrar,
- 26 S.: The importance of transport model uncertainties for the estimation of CO<sub>2</sub> sources and sinks
- 27 using satellite measurements, Atmos. Chem. Phys., 10, 9981-9992, doi:10.5194/acp-10-9981-
- 28 2010, 2010.



- 1 Jung, M., Reichstein, M., Bondeau, A.: Towards global empirical upscaling of FLUXNET eddy  
2 covariance observations: validation of a model tree ensemble approach using a biosphere model,  
3 Biogeosciences, 6, 2001–2013, doi:10.5194/bg-6-2001-2009, 2009.
- 4 Jung, M., Henkel, K., Herold, M. and Churkina, G.: Exploiting synergies of global land cover  
5 products for carbon cycle modeling, Remote Sensing of Environment, 101(4), 534–553,  
6 doi:10.1016/j.rse.2006.01.020, 2006.
- 7 Kaminski, T. and Heimann, M.: A coarse grid three-dimensional global inverse model of the  
8 atmospheric transport 1. Adjoint model and Jacobian matrix, J. Geophys. Res. 104, D15, 18,535–  
9 18,553, doi: 10.1029/1999JD900147, 1999a.
- 10 Kaminski, T., Heimann, M. and Giering, R.: A coarse grid three-dimensional global inverse  
11 model of the atmospheric transport: 2. Inversion of the transport of CO<sub>2</sub> in the 1980s, J.  
12 Geophys. Res.: Atmospheres (1984--2012) 104, D15, 18,555–18,581, doi:  
13 10.1029/1999JD900146, 1999b.
- 14 Kaminski, T., Rayner, P. J., Voßbeck, M., Scholze, M. and Koffi, E.: Observing the continental-  
15 scale carbon balance assessment of and sampling complementarity and redundancy in a  
16 terrestrial and assimilation system by means of quantitative network design, Atmos. Chem. and  
17 Phys. 12, 7867–7879, doi: 10.5194/acp-12-7867-2012, 2012.
- 18 Kountouris, P., Gerbig, C., Rödenbeck, C., Karstens, U., Koch, F. Th., Heimann, M.:  
19 Atmospheric CO<sub>2</sub> inversions at the mesoscale using data driven prior uncertainties. Part2: the  
20 European terrestrial CO<sub>2</sub> fluxes, submitted to Atmos. Chem. Phys.
- 21 Kountouris, P., Gerbig, C., Totsche, K. U., Dolman, A. J., Meesters, A. G. C. A., Broquet, G.,  
22 Maignan, F., Gioli, B., Montagnani, L., Helfter, C.: An objective prior error quantification for  
23 regional atmospheric inverse applications, Biogeosciences, 12, 7403–7421, doi: 10.5194/bg-12-  
24 7403-2015, 2015.
- 25 Lauvaux, T., Schuh, A. E., Bocquet, M., Wu, L., Richardson, S., Miles, N. and Davis, K. J.:  
26 Network design for mesoscale inversions of CO<sub>2</sub> sources and sinks, Tellus B 64, 17980, doi:  
27 10.3402/tellusb.v64i0.17980, 2012.



- 1 Lauvaux, T., Uliasz, M., Sarraz, C., Chevallier, F., Bousquet, P., Lac, C., Davis, K., Ciais, P.,  
2 Denning, A. and Rayner, P.: Mesoscale inversion: first results from the CERES campaign with  
3 synthetic data, Atmos. Chem. and Phys., 8, 3459-3471, doi:10.5194/acp-8-3459-2008, 2008.
- 4 Lin, J. C., and C. Gerbig: Accounting for the effect of transport errors on tracer inversions,  
5 Geophys. Res. Lett., 32, L01802, doi:10.1029/2004GL021127, 2005.
- 6 Lin, J. C., Gerbig, C., Wofsy, S. C., Andrews, A. E., Daube, B. C., Davis, K. J., and Grainger, C.  
7 A.: A near-field tool for simulating the upstream influence of atmospheric observations: The  
8 Stochastic Time-Inverted Lagrangian Transport (STILT) model, J. Geophys. Res., 108, 4493,  
9 doi: 10.1029/2002JD003161, 2003
- 10 Lokupitiya, R. S., Zupanski, D., Denning, A. S., Kawa, S. R., Gurney, K. R. and Zupanski, M.:  
11 Estimation of global CO<sub>2</sub> fluxes at regional scale using the maximum likelihood ensemble filter,  
12 J. Geophys. Res. 113, D20110, doi: 10.1029/2007JD009679, 2008.
- 13 Mahadevan, P., Wofsy, S. C., Matross, D. M., Xiao, X., Dunn, A. L., Lin, J. C., Gerbig, C.,  
14 Munger, J. W., Chow, V. Y. and Gottlieb, E. W.: A satellite-based biosphere parameterization  
15 for net ecosystem CO<sub>2</sub> exchange: Vegetation Photosynthesis and Respiration Model (VPRM),  
16 Glob. Biogeochem. Cy. 22, GB2005, doi: 10.1029/2006GB002735, 2008.
- 17 Meesters, A. G. C. A., Tol, L. F., Peters, W., Hutjes, R. W. A., Vellinga, O. S., Elbers, J. A.,  
18 Vermeulen, A. T., van der Laan, S., Neubert, R. E. M., Meijer, H. A. J., Dolman, A. J.: Inverse  
19 carbon dioxide flux estimates for the Netherlands, J. Geophys. Res.-Atmos. 117, D20306, 1984-  
20 2012, doi: 10.1029/2012jd017797, 2012.
- 21 Michalak, A., M., Bruhwiler L. and Tans, P. P.: A geostatistical approach to surface flux  
22 estimation of atmospheric trace gases, J. Geophys. Res. 109, D14109, doi:  
23 10.1029/2003JD004422, 2004.
- 24 Michalak, A., Hirsch, A., Bruhwiler, L., Gurney, K. R., Peters, W., and Tans, P. P.: Maximum  
25 likelihood estimation of covariance parameters for Bayesian atmospheric trace gas surface flux  
26 inversions, J. Geophys. Res., 100, D24107, doi:10.1029/2005JD005970, 2005.



- 1 Mueller, K. L., Gourdji, S. M. and Michalak, A. M.: Global monthly averaged CO<sub>2</sub> fluxes  
2 recovered using a geostatistical inverse modeling approach: 1. Results using atmospheric  
3 measurements, *J. Geophys. Res.* 113, D21114, doi: 10.1029/2007JD009734, 2008.
- 4 Peters, W., Jacobson, A. R., Sweeney, C., Andrews, A. E., Conway, T. J., Masarie, K., B. Miller,  
5 J., Bruhwiler, L. M. P., Petron, G., Hirsch, A. I., Worthy, D. E. J., van der Werf, G. R.,  
6 Wennberg, J. T. R. P. O., Krol, M. C. and Tans, P. P.: An atmospheric perspective on North  
7 American carbon dioxide exchange: CarbonTracker, *Proceedings of the National Academy of*  
8 *Sciences*, 104, 48, 18,925-18,930, doi: 10.1073/pnas.0708986104, 2007.
- 9 Peylin, P., Law, R. M., Gurney, K. R., Chevallier, F., Jacobson, A. R., Maki, T., Niwa, Y., Patra,  
10 P. K., Peters, W., Rayner, P. J., Rödenbeck, C., van der Laan-Luijkx, I. T., and Zhang, X.:  
11 Global atmospheric carbon budget: results from an ensemble of atmospheric CO<sub>2</sub> inversions,  
12 *Biogeosciences* 10, 6699-6720, doi: 10.5194/bg-10-6699-2013, 2013.
- 13 Peylin, P., Houweling, S., Krol, M. C., Karstens, U., Rödenbeck, C., Geels, C., Vermeulen, A.,  
14 Badawy, B., Aulagnier, C., PREGGER, T., Delage, F., Pieterse, G., Ciais, P., and Heimann, M.:  
15 Importance of fossil fuel emission uncertainties over Europe for CO<sub>2</sub> modeling: model  
16 intercomparison, *Atmos. Chem. Phys.*, 11, 6607-6622, doi:10.5194/acp-11-6607-2011, 2011.
- 17 Peylin, P., Rayner, P., Bousquet, P., Carouge, C., Hourdin, F., Heinrich, P., Ciais, P. and  
18 AEROCARB contributors: Daily CO<sub>2</sub> flux estimates over Europe from continuous atmospheric  
19 measurements: 1, inverse methodology, *Atmos. Chem. Phys.* 5, 3173-3186, doi:10.5194/acp-5-  
20 3173-2005, 2005.
- 21 Rayner, P. J., Scholze, M., Knorr, W., Kaminski, T., Giering, R. and Widmann, H.: Two decades  
22 of terrestrial carbon fluxes from a carbon cycle data assimilation system (CCDAS), *Glob.*  
23 *Biogeochem. Cy.* 19, GB2026, doi: 10.1029/2004GB002254, 2005.
- 24 Rivier, L., Peylin, P., Ciais, P., Gloor, M., Roedenbeck, C., Geels, C., Karstens, U., Bousquet, P.,  
25 Brandt, J. and Heimann, M.: European CO<sub>2</sub> fluxes from atmospheric inversions using regional  
26 and global transport models, *Climatic Change*, 103, 93-115, doi: 10.1007/s10584-010-9908-4,  
27 2010.



- 1 Rödenbeck C., Houwelling S., Gloor M. and Heinmann, M.: CO<sub>2</sub> flux history 1982-2001
- 2 inferred from atmospheric data using a global inversion of atmospheric transport, Atmos. Chem.
- 3 and Phys. 3, 1919-1964, doi: 10.5194/acp-3-1919-2003, 2003.
- 4 Rödenbeck, C.: Estimating CO<sub>2</sub> sources and sinks from atmospheric mixing ratio measurements
- 5 using a global inversion of atmospheric transport, Technical Report 6, Max Planck Institute for
- 6 Biogeochemistry, Jena, <http://www.bgc-jena.mpg.de/mpg/websiteBiogeochemie/>
- 7 Publikationen/Technical Reports/tech report6.pdf, 2005.
- 8 Rödenbeck, C., Gerbig, C., Trusilova, K. and Heimann, M.: A two-step scheme for high-
- 9 resolution regional atmospheric trace gas inversions based on independent models, Atmos.
- 10 Chem. and Phys. 9, 5331-5342, doi:10.5194/acp-9-5331-2009, 2009.
- 11 Rödenbeck, C., Bakker, D. C. E., Metzl, N., Olsen, A., Sabine, C., Cassar, N., Reum, F.,
- 12 Keeling, R. F. and Heimann, M.: Interannual sea-air CO<sub>2</sub> flux variability from an observation-
- 13 driven ocean mixed-layer scheme, Biogeosciences, 11(17), 4599–4613, doi:10.5194/bg-11-4599-
- 14 2014-supplement, 2014.
- 15 Schuh, A. E., Denning, A. S., Corbin, K. D., Baker, I. T., Uliasz, M., Parazoo, N., Andrews, A.
- 16 E. and Worthy, D. E. J.: A regional high-resolution carbon flux inversion of North America for
- 17 2004, Biogeosciences, 7, 1625-1644 , doi: 10.5194/bg-7-1625-2010, 2010.
- 18 Schuh, A. E., Denning, A. S., Uliasz, M. and Corbin, K. D.: Seeing the forest through the trees:
- 19 Recovering large-scale carbon flux biases in the midst of small-scale variability, J. Geophys
- 20 Res., 114, doi: 10.1029/2008JG000842, 2009.
- 21 Schulze, E. D., Ciais, P., Luyssaert, S., Schrumpf, M., Janssens, I. A., Thiruchittampalam, B.,
- 22 Theloke, J., Saurat, M., Bringezu, S., Lelieveld, J., Lohila, A., Rebmann, C., Jung, M.,
- 23 Bastviken, D., Abril, G., Grassi, G., Leip, A., Freibauer, A., Kutsch, W., Don, A., Nieschulze, J.,
- 24 Börner, A., Gash, J. H., and Dolman, A. J.: The European carbon balance. Part 4: integration of
- 25 carbon and other trace-gas fluxes, Glob. Change Biology, 16, 1451-1469, doi: 10.1111/j.1365-
- 26 2486.2010.02215.x, 2010.



- 1 Thompson, R. L., Gerbig, C. and Rödenbeck, C.: A Bayesian inversion estimate of N<sub>2</sub>O  
2 emissions for western Europe and the assessment of aggregation errors, Atmos. Chem. Phys., 11,  
3 3443-3458, doi: 10.5194/acp-11-3443-2011, 2011.
- 4 Tolk, L. F., Dolman, A. J., Meesters, A. G. C. A. and Peters, W.: A comparison of different  
5 inverse carbon flux estimation approaches for application on a regional domain, Atmos. Chem.  
6 Phys., 11, 10349-10365, doi: 10.5194/acp-11-10349-2011, 2011.
- 7 Trusilova, K., Rödenbeck, C., Gerbig, C., and Heinmann, M.: Technical Note: A new coupled  
8 system for global to regional downscaling of CO<sub>2</sub> concentration estimation, Atmos. Chem. Phys.  
9 10, 3205-3213, doi:10.5194/acp-10-3205-2010, 2010.
- 10 Trusilova, K., and Churkina, G.: The Terrestrial Ecosystem Model GBIOME-BGCv1, Max-  
11 Planck Institute for Biogeochemistry, Technical Report 14, [http://www.db-](http://www.db-thueringen.de/servlets/DerivateServlet/Derivate-20689/tech_report14.pdf)  
12 [thueringen.de/servlets/DerivateServlet/Derivate-20689/tech\\_report14.pdf](http://www.db-thueringen.de/servlets/DerivateServlet/Derivate-20689/tech_report14.pdf), 2008.
- 13 Zupanski, D., Denning, A. S., Uliasz, M., Zupanski, M., Schuh, A. E., Rayner, P. J., Peters, W.  
14 and Corbin, K. D.: Carbon flux bias estimation employing Maximum Likelihood Ensemble Filter  
15 (MLEF), J. Geophys. Res., 112, D17107, doi: 10.1029/2006JD008371, 2007.





1 Table 1. Optimized VPRM parameters  $SW_0$ ,  $\lambda_{SW}$ ,  $\alpha$ ,  $\beta$  for different vegetation classes<sup>a</sup>

	$SW_0$	$\lambda_{SW}$	$\alpha$	$\beta$
Evergreen forest	275	0.226	0.288	-1.10
Deciduous forest	254	0.215	0.181	0.84
Mixed forest	446	0.163	0.244	-0.49
Open shrub	70	0.293	0.055	-0.12
Crop	1132	0.086	0.092	0.29
Grass	528	0.119	0.125	0.017

2 <sup>a</sup>Units are as follows:  $SW_0$ :  $W\ m^{-2}$ ;  $\lambda_{SW}$ :  $\mu\text{mole CO}_2\ m^{-2}s^{-1} / (W\ m^{-2})$ ;  $\alpha$ :  $\mu\text{mole CO}_2\ m^{-2}s^{-1} / ^\circ C$ ;  
 3  $\beta$ : ( $\mu\text{mole CO}_2\ m^{-2}s^{-1}$ ).

4



- 1 Table 2. Information on the stations used for the regional inversions. Same network applied for
- 2 the synthetic, and the real data inversions in Kountouris et al. (2016). In first column the term
- 3 “type” stands for continuous (C) or flask (F) data.

Site Code / type	Name	Latitude ( ° )	Longitude ( ° )	Height (m.a.s.l.) (m)	Measurement height (above ground) (m)	Model height
BAL/F	Baltic Sea, Poland	55.50	16.67	8	57	28
BIK/C	Bialystok, Poland	53.23	23.03	183	90	90
CBW/C	Cabauw, Netherlands	51.58	4.55	-2	200	200
CMN/C	Monte Cimone, Italy	44.18	10.7	2165	12	670
HEI/C	Heidelberg, Germany	49.42	8.67	116	30	30
HPB/F	Hohenpeissenberg, Germany	47.80	11.01	934	50	10
HUN/C	Hegyhatsal, Hungary	46.95	16.65	248	115	96
JFJ/C	Jungfrauoch, Switzerland	46.55	7.98	3572	10	720
KAS/C	Kasprowy Wierch	49.23	19.93	1987	5	480
LMU/C	La Muela, Spain	41.36	-1.6	570	79	80
MHD/C	Mace Head, Ireland	53.33	-9.90	25	10	15
OXK/C	Ochsenkopf,	50.03	11.81	1022	163	163



	Germany						
PRS/C	Plateau	Rosa,	45.93	7.71	3480	-	500
	Italy						
PUY/C	Puy De	Dome,	45.77	2.97	1465	10	400
	France						
SCH/C	Schauinsland,		47.92	7.92	1205	-	230
	Germany						
WES/C	Westerland,		54.93	8.32	12	-	15
	Germany						



1 Table 3. RMSD (first column in ppm) and correlation coefficients (second column) between  
 2 known truth and prior/posterior CO<sub>2</sub> dry mole fractions for daily “daytime” or “nighttime”  
 3 averaged values and for each station. The third column shows  $\chi^2$ , the normalized dry mole  
 4 fraction mismatch per degree of freedom for 7-day averaged residuals, as a measure of how well  
 5 the data were fitted. The format for each station is as follows: RMSD |  $r^2$  |  $\chi^2$ .

	Prior	B1	S1
BAL	4.78   0.07   18.44	0.89   0.97   0.48	1.02   0.96   0.37
BIK	5.28   0.43   15.50	1.20   0.97   0.18	1.29   0.97   0.25
CBW	8.60   0.04   74.29	0.99   0.99   1.31	1.06   0.99   1.34
CMN	2.68   0.33   6.31	0.74   0.93   0.08	0.78   0.92   0.10
HEI	11.39   0.37   12.97	1.83   0.98   0.36	1.84   0.98   0.37
HPB	7.73   0.35   26.58	1.01   0.99   0.21	1.19   0.99   0.31
HUN	6.50   0.63   31.89	1.36   0.98   0.21	1.46   0.98   0.25
JFJ	3.12   0.21   3.93	1.24   0.86   0.24	1.31   0.84   0.27
KAS	4.00   0.32   10.67	0.73   0.98   0.11	0.80   0.97   0.15
LMU	3.42   0.19   6.5	0.79   0.95   0.12	0.86   0.94   0.16
MHD	1.53   0.0002   0.83	0.65   0.09   0.16	0.68   0.06   0.17
OXK	6.10   0.21   38.50	3.35   0.76   0.76	3.40   0.75   0.80
PRS	2.32   0.15   2.46	0.70   0.92   0.30	0.74   0.91   0.33
PUY	4.27   0.15   12.06	0.68   0.97   0.06	0.73   0.15   0.09
SCH	4.76   0.26   21.17	0.90   0.97   0.07	0.95   0.97   0.09

6

7

8

9

10

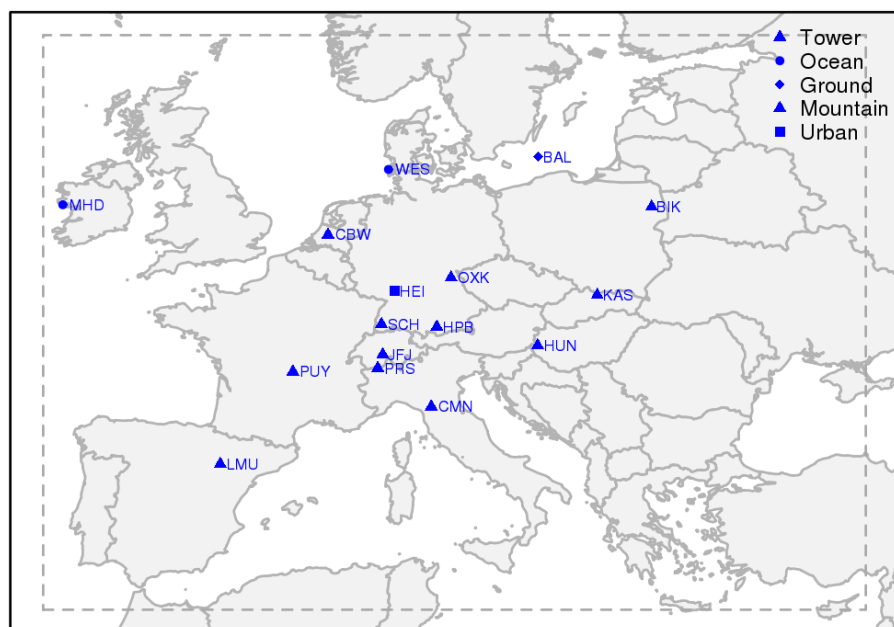
11



- 1 Table 4. Performance of the two error structures expressed as the spatial RMSD of the optimized
- 2 monthly and annual NEE fluxes compared to the truth for the whole domain in  $\mu\text{mole m}^{-2} \text{s}^{-1}$ .

	Annual	JAN	FEB	MAR	APR	MAY	JUN	JUL	AUG	SEP	OCT	NOV	DEC
prior	0.38	0.61	0.53	0.55	1.06	1.26	1.56	1.17	0.94	0.65	0.57	0.63	0.63
B1	0.33	0.46	0.40	0.45	0.84	0.99	1.21	1.00	0.86	0.63	0.43	0.46	0.44
S1	0.34	0.48	0.41	0.45	0.86	1.01	1.24	1.03	0.86	0.63	0.45	0.47	0.45

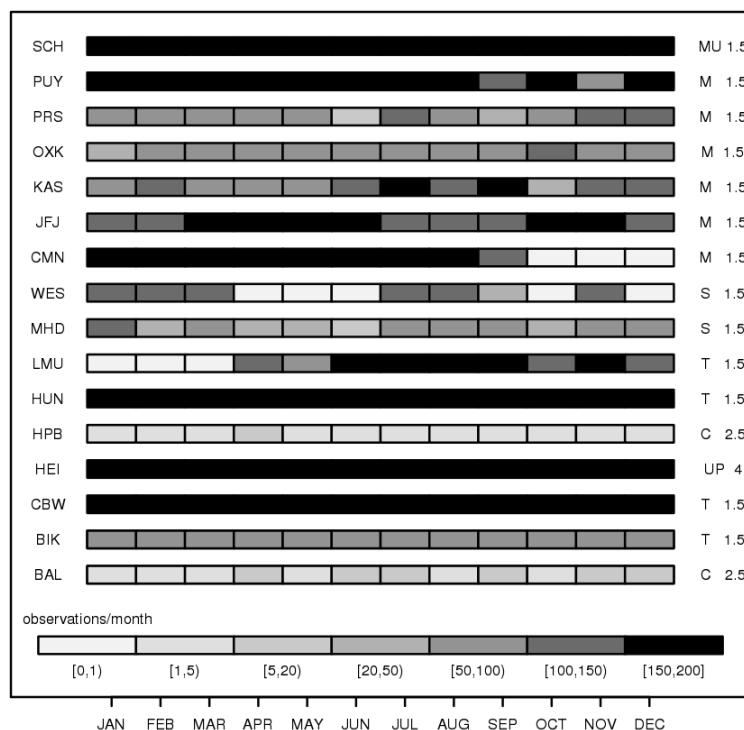
3



1

2 Figure 1. Domain of the inversions (dashed rectangle). Locations of the atmospheric  
 3 measurement stations are shown with blue marks. Red stars denote the eddy covariance locations  
 4 used for flux comparisons at grid scale.

5



1

2 Figure 2. Monthly data coverage plot for the atmospheric stations used in the regional inversions.  
 3 Left column shows the code name and the right columns show the station class and the assigned  
 4 uncertainty in units of ppm. “C” stands for continental sites near the surface, “T” for continental  
 5 tall towers, “S” for stations near shore, “M” for mountain sites, “MU” for mountain sites with  
 6 diurnal upslope winds and “UP” for urban pollutant.

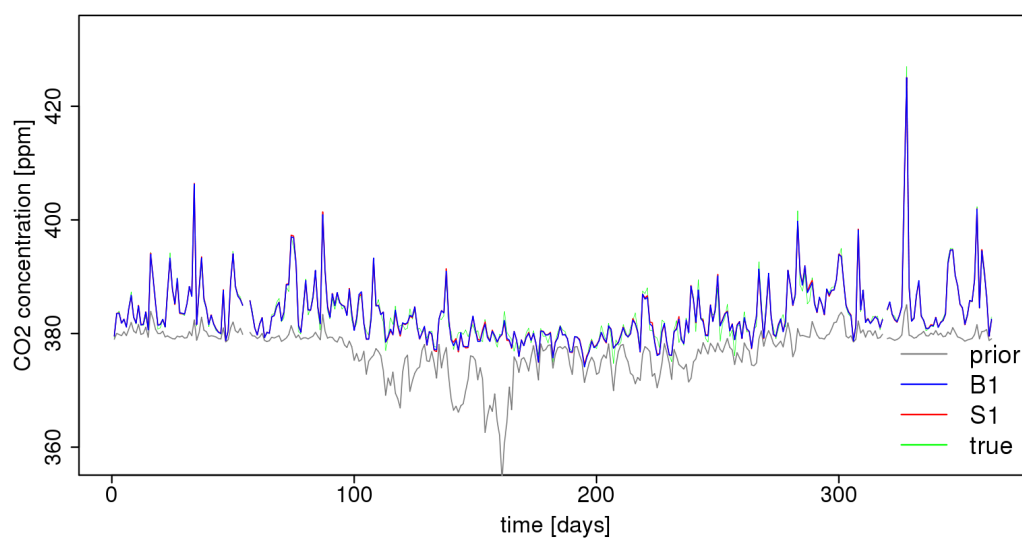
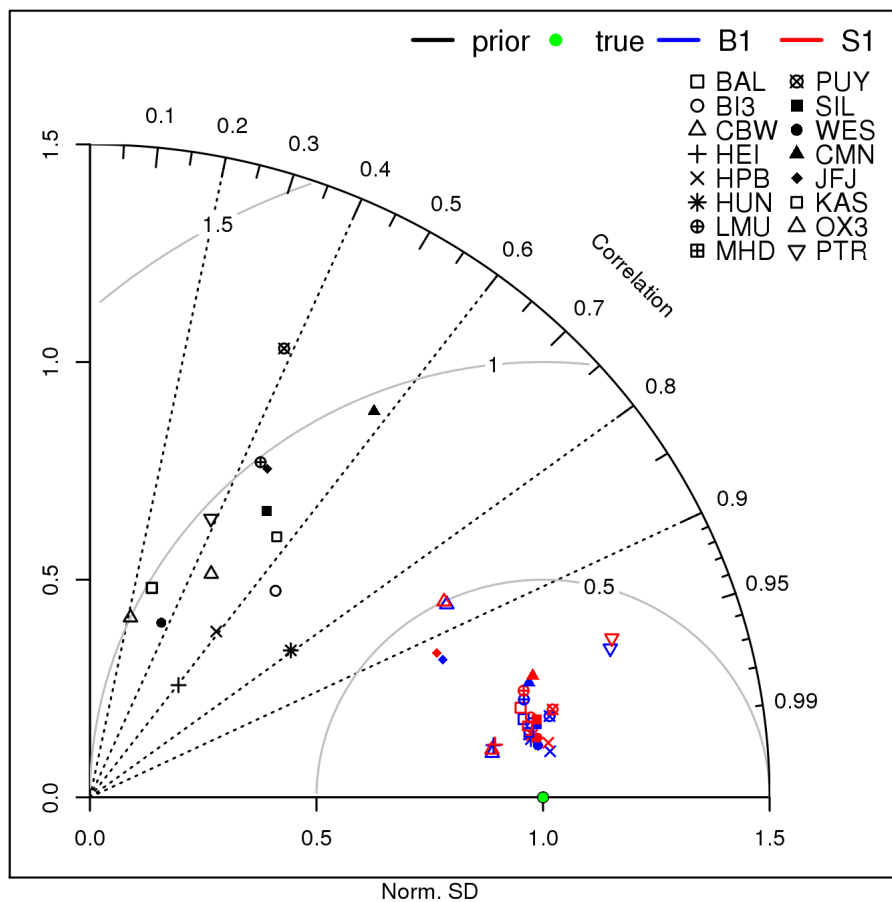
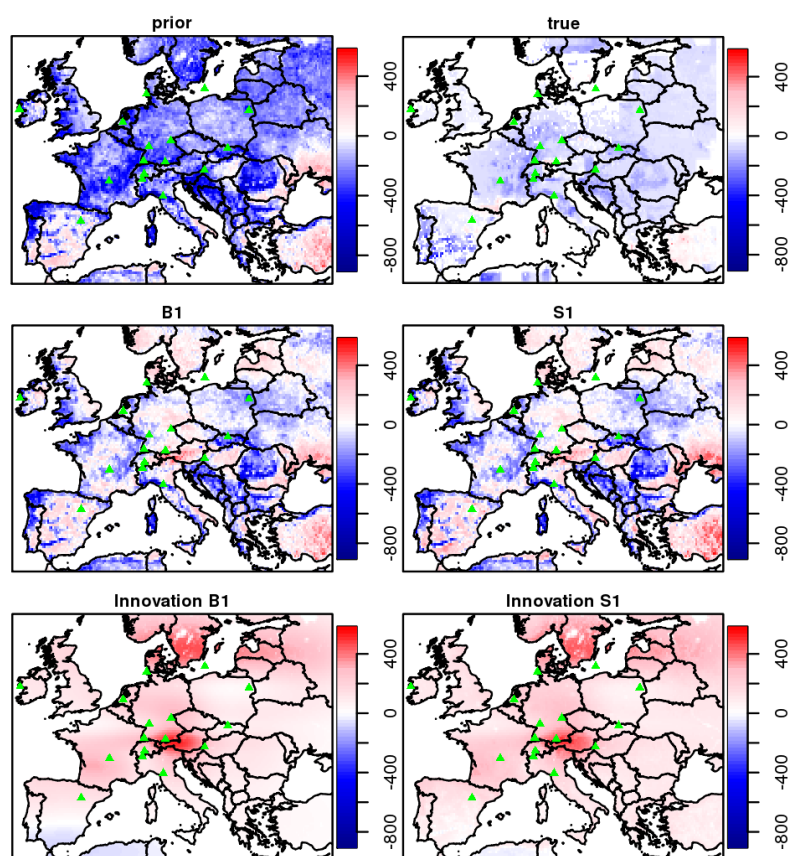


Figure 3. Daily nighttime (23:00–4:00 UTC) averages for prior, true, and posterior CO<sub>2</sub> dry mole fraction time series for the mountain site Schauinsland. Time starts at 1<sup>st</sup> January 2007.



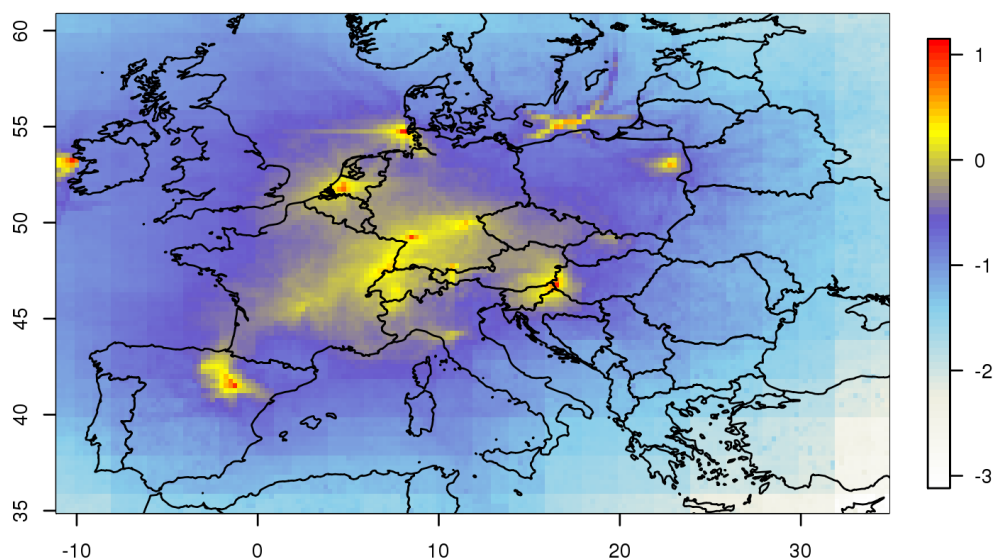


1  
 2 Figure 4. Taylor diagram for modeled and measured time-series of CO<sub>2</sub> dry mole fractions. Prior  
 3 (black), true (green, the perfect match of modeled and true time-series) and the different  
 4 inversion cases (R0 blue; R1 red) are displayed. Different symbols denote different atmospheric  
 5 stations. The normalized SD was calculated as the ration of the SD of the modeled time-series to  
 6 the SD of observations.

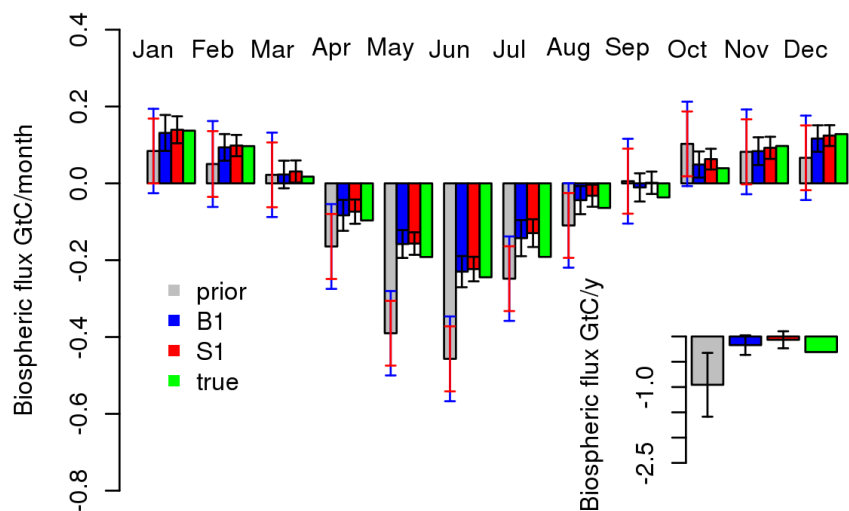


1

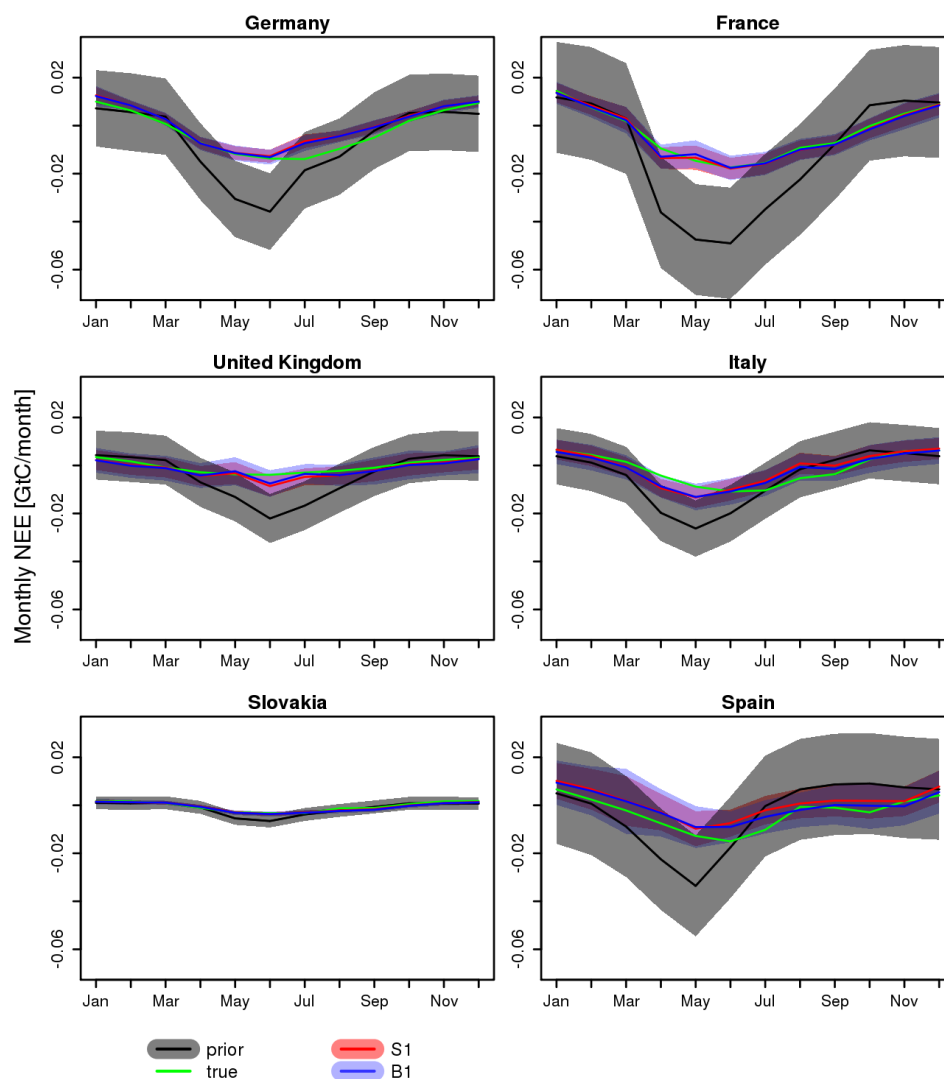
2 Figure 5. Annual spatial distribution for the prior, true, and posterior biogenic flux estimates for  
 3 the two synthetic inversions S1 and B1 (top two rows), and flux innovation defined as the  
 4 difference posterior - prior (bottom row). Fluxes are given in units of  $\text{gCy}^{-1}\text{m}^{-2}$ .



1  
 2 Figure 6. Annual integrated influence for 2007 of the current atmospheric network. Footprint  
 3 influence is presented in a logarithmic scale and units are in  $\log_{10}[\text{ppm}/(\mu\text{mol}/\text{m}^2/\text{s})]$



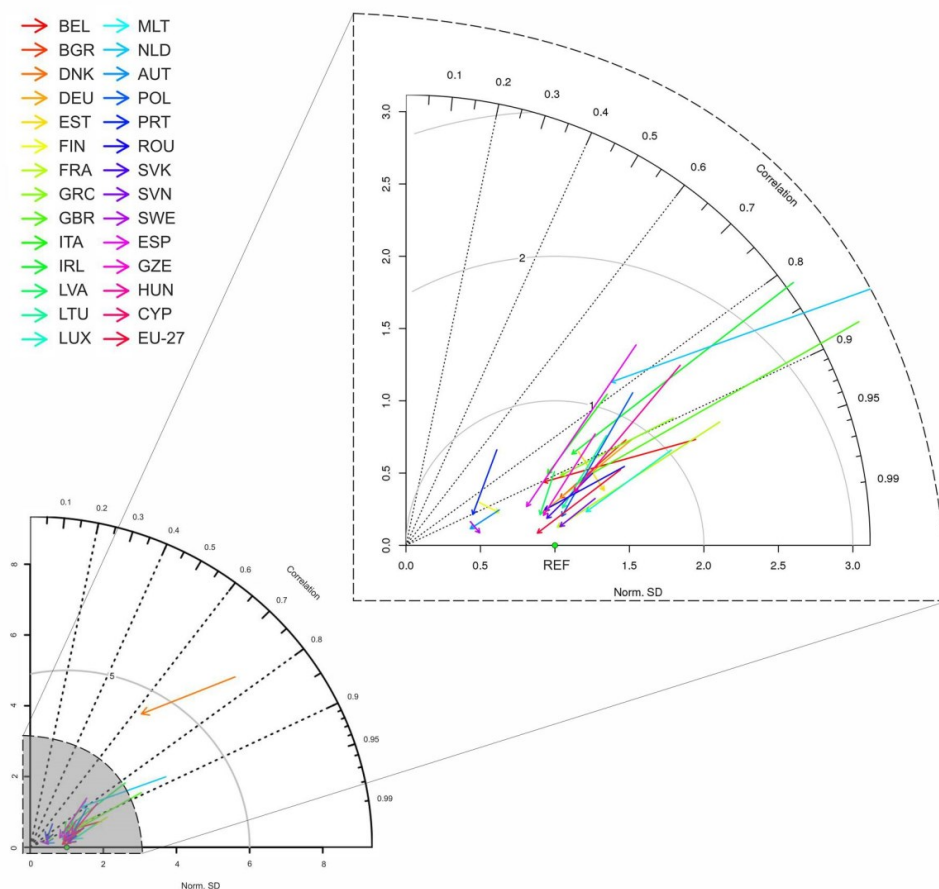
1  
 2 Figure 7. Monthly and annual carbon flux budget, integrated over the European domain. Note  
 3 that both inversions share the same annual prior uncertainty but monthly uncertainties differ.  
 4 Blue and red error bars denote the prior uncertainty for the B1 and S1 scenarios respectively.  
 5



1

2 Figure 8. Temporal evolution of monthly NEE for selected European countries for the synthetic  
 3 data inversion.

4



1  
 2 Figure 9. Overview of the model performance summarized in a Taylor diagram. Posterior and prior  
 3 monthly and country scale aggregated biospheric fluxes are compared against the reference fluxes  
 4 (“true”). Each line corresponds to a different country. The starting point of each arrow shows  
 5 prior/reference comparison and the ending point the posterior/reference comparison. Ideally the ending  
 6 point should coincide with the green point which represents the reference model.

7  
 8  
 9  
 10  
 11

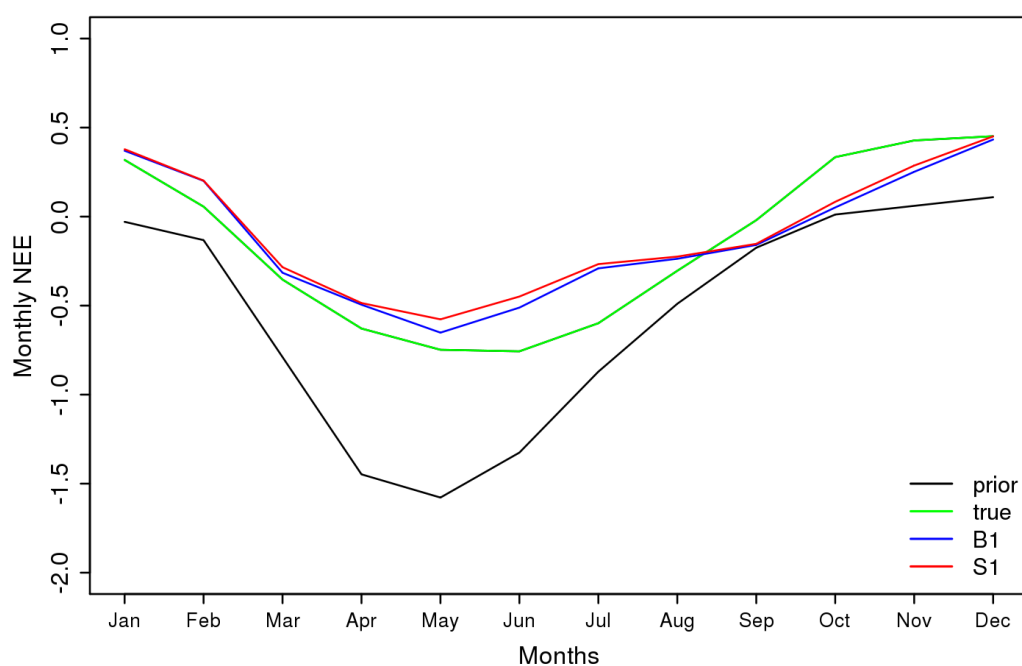


Figure 10. Mean monthly NEE averaged over the 53 different eddy covariance site locations as reported in Kountouris et al. (2015). A priori (black), true (green), and posterior fluxes for scenarios B1 (blue) and S1 (red) are shown. Units are in  $\text{gCm}^{-2}\text{day}^{-1}$ .

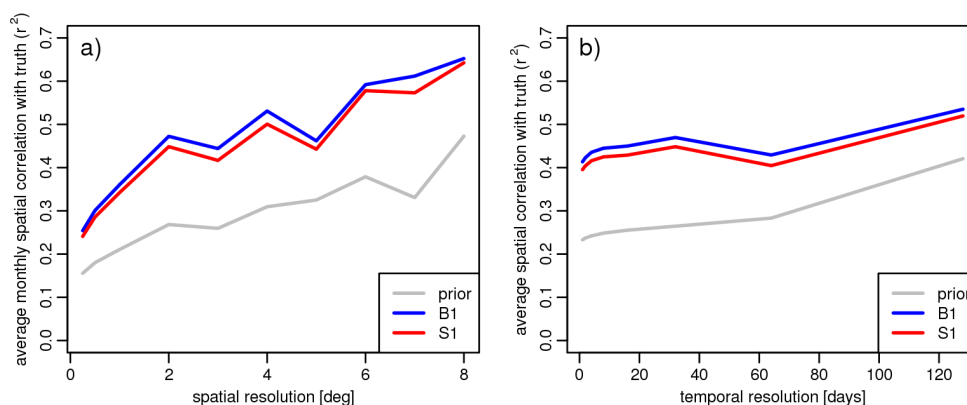


Figure 11. a): Mean spatial correlation of monthly fluxes with true fluxes as function of spatial flux aggregation scale for prior fluxes (grey), and for posterior fluxes from scenarios B1 (blue) and S1 (red). b): Mean spatial correlation of fluxes with true fluxes at 2 deg. spatial resolution as function of temporal flux aggregation scale for prior fluxes (grey), and for posterior fluxes from scenarios B1 (blue) and S1 (red).